Computational design of a single crystal nickel-based superalloy with improved specific creep endurance at high temperature

Edern Menou, Jérémy Rame, Clara Desgranges, Gérard Ramstein, Franck Tancret

Version of Record: https://www.sciencedirect.com/science/article/pii/S0927025619304938
Manuscript_16f338d8685f4e1734a4edc3dd597a38

Computational design of a single crystal nickel-based superalloy with improved specific creep endurance at high temperature

Edern Menou[a,b,c], Jérémy Rame[c], Clara Desgranges[c], Gérard Ramstein[b], Franck Tancret[a]

[a] *Institut des Matériaux Jean Rouxel (IMN), CNRS UMR 6502, Université de Nantes, 2 rue de la Houssinière, BP 32229, 44322 Nantes Cedex 3, France*
[b] *Laboratoire des Sciences du Numérique de Nantes (LS2N), CNRS UMR 6004, Université de Nantes, Rue Christian Pauc, BP 50609, 44306 Nantes Cedex 3, France*
[c] *Safran Tech, Materials and Processes Department, Rue des Jeunes Bois, Châteaufort, 78114 Magny-les-Hameaux, France*

Abstract

A Gaussian process regression model for estimating the creep rupture stress of single crystal nickel-based superalloys is constructed. It is built and validated on data disclosed in patents as well as scientific and technical reports. This model is coupled with computational thermodynamics for the prediction of microstructural features, and a model for the estimation of density. Using this combination, the key characteristics of a large number of potential alloys are systematically computed as a function of their composition. Materials specifications targeted towards applications as turbine blades, which none of the alloys from the creep database follow, narrow down the search from 300 000 000 to 180 000 alloys. A large number of these candidates are predicted as featuring greater specific properties than existing single crystal nickel-based superalloys. The selection criteria used to isolate alloys for experimental validation are discussed, and lead to several alloys displaying good agreement between their predicted microstructure and estimated properties.

Keywords: CALPHAD; Thermo-Calc; optimisation; artificial intelligence; machine learning

1. Introduction

The design of new nickel-based superalloys, while stimulated by the need for competitive high-temperature materials in the aerospace and power generation industries, is hindered by its complexity. The exceptional high-temperature properties of these materials arise from the combination of numerous alloying elements in possibly large concentrations, meaning a gigantic number of alloys can be enumerated. As an example of this combinatorial complexity, consider a popular single crystal nickel-based superalloy designed for use in the hot sections of gas turbines such as CMSX-4+ [1]. This alloy contains up to 9 alloying elements whose maximal concentration can reach 10 wt.%. Varying its alloying content solely within the boundaries of its patent generates roughly 10^6 alloys using an accuracy of 0.1 wt.%!

To avoid the tedious trial-and-error design process, methods have been proposed to design superalloys that rely on models describing properties as a function of composition and processing [2–7]. For instance, the method of computer-coupling of phase diagrams and thermochemistry (CALPHAD) has notably made it possible to estimate an alloy constitution at high-temperature equilibrium (i.e. stable phases proportion and composition) as a function of its nominal composition. The method has been employed in a number of works [6–14].

Yet, with regards to alloy design, predicting constitution is insufficient as it only partially prefigures of the actual material behaviour. In the case of the nickel-based superalloys, more precise information is needed regarding their thermomechanical properties. Such properties relate in non-linear ways to composition making the construction of holistic physical models still beyond reach. Data mining-based statistical modelling has been shown to be able to provide these correlations between composition and properties. Tools such as artificial neural networks or Gaussian processes can indeed quantify the influence of variations of input variables (e.g. alloying elements) on an output (e.g. yield stress) provided sufficient data which comprises the boundaries of said variations has been gathered. The mining of relationships encoded in existing data using these techniques has been widely executed in the past twenty years to model a variety of macroscopic properties as a

Email address: franck.tancret@univ-nantes.fr (Franck Tancret)

function of composition with the goal of designing superalloys with improved performance [2, 4, 7, 12, 15–25].

Whereas, in this context, the modelling of creep deformation behaviour of the polycrystalline nickel-based superalloys using data mining has already been successfully exploited [3, 7, 12, 22], that of the single crystal nickel-based superalloys has received less attention until then. Physical models have been devised but these are generally either based or validated on a limited set of data points thus seeing their extrapolation capabilities only locally challenged [6, 9, 26]. However, such models should explicitly account for the dependency of creep deformation on composition if they are to be used for compositional optimisation. A recent significant contribution towards this objective is found in the work of Sulzer and Reed [27] who have yet to exploit their composition-dependent creep merit index.

It is the purpose of this work to report both on the development of a Gaussian process model for the prediction of creep rupture stress and on its exploitation, together with physicochemical models, with the aim of designing single crystal nickel-based superalloys. This work is motivated by the significant probability of finding superalloys with improved properties (or combinations thereof) as the space of all possible alloys has only been scarcely explored to date. The paper first introduces the metallurgy of these materials before delving into the different models used to design new ones. The design specifications and the results of the exploitation are then presented, and a discussion of the most important results is proposed.

2. Background

The single crystal nickel-based superalloys are widely used for the manufacture of blades and vanes for the hot sections of gas turbines. Their service conditions are harsh: they are exposed to the high temperatures of the gas stream, with blades being subjected to significant centrifugal stresses generated by large rotational speeds. Alloying with numerous elements has proven to be effective at slowing down the rate of mechanical and chemical degradation.

High temperature mechanical resistance of mainstream single crystal nickel-based superalloys is primarily conferred by a dual phase microstructure with Ni_3Al-type γ' precipitates embedded in a disordered face-centered cubic matrix (γ). This allows the use of both solid solution strengthening and precipitation hardening effects. Significant solid solution strengthening occurs when substituting base elements in both phases with elements such as molybdenum, niobium, rhenium, tantalum or tungsten, which pin the dislocations and decrease the rate of creep damaging. The precipitation of γ' particles further contributes to this dislocation impairment at higher temperature because its softening is limited compared to that of the matrix. The resistance to creep is also enhanced when the γ' content is capped at around 70 mol.% [28] and when the γ and γ' phases are coherent, i.e. the relative difference between their lattice parameters (termed lattice misfit) is limited [29]. This misfit is notably dependent on the partitioning of alloying elements between the two phases.

This microstructure is controlled via heat treatments generally involving a solution treatment followed by aging in the γ/γ' phase field to achieve the targeted γ' precipitates size. In this regard, the γ' content and that of various elements are key in ensuring that a window of solutionising exists below the alloy solidus and that the alloy is thus processable.

Better mechanical resistance of blades can also be achieved by lowering the superalloy volumetric mass density because it factors in the calculation of centrifugal stresses. This goes against adding heavy elements, i.e. an effective compromise between weight and strength must be found in addition to the aforementioned criteria.

Single crystal nickel-based superalloys can operate either uncoated or coated. In the former case, resistance to corrosion and oxidation is imparted most notably by additions of aluminium and chromium which, together with reactive elements such as hafnium, manganese and silicon, contribute to the formation and adherence of continuous protective oxide layers at the interface between the alloy and its environment. Most oxidation-resistant single crystal nickel-based superalloys are in fact alumina-formers, naturally forming a layer of Al-rich oxides. This assumes enough "free" aluminium remains in the (γ) matrix to diffuse outward, a freedom possibly contested by the precipitation of the Al-rich γ' phase. When the service temperature is such that the resistance of uncoated blades is compromised, Thermal Barrier Coatings (TBC) are added. These barriers effectively reduce the temperature at the surface of the blades. However, the TBC may over time be subject to spallation; it is thus crucial the resistance to corrosion of the superalloy itself be sufficient.

Alloying also impacts castability, i.e. the ability of the material to be manufactured through investment casting without defect. Localised growth of equiaxed grains, termed freckles, is one of these defects degrading creep endurance. It is linked to high amounts of rhenium and tungsten which uneven the density balance between the liquid and solid phases during cooling.

Excessive alloying can be detrimental as it exacer-

bates the risk of promoting the formation of deleterious phases. Most notably, high contents of chromium and molybdenum favours the precipitation of the brittle Topologically Closed-Packed (TCP) phases. Large amounts of TCP phases negate the potential solid solution strengthening effect of these elements and lessen the overall mechanical strength by providing preferential cracking sites.

It is apparent from these considerations that a careful crafting of the composition and microstructure is mandatory to reach an optimal combination of properties.

3. Models and design criteria

The following subsections offer insights into the models and criteria which are to provide estimates of key characteristics of the single crystal nickel-based superalloys.

3.1. Creep resistance

Gaussian processes regression (also known as "kriging") is used to model the dependencies of the creep rupture stress of superalloys on their composition.

Gaussian processes are a supervised learning method allowing regression over an output as a function of multiple inputs. Such model is learnt from data, i.e. it assumes a consistent aggregation of data in the form of databases has been conducted. At the core of Gaussian processes lies the covariance function, which incorporates a measure of the distance between data points in the input space, and is used to estimate the value of an output given a new input by interpolation. Due to the flexible nature of the covariance function [30], Gaussian processes are able to capture nonlinear relationships in the data. Furthermore, predictions from Gaussian processes are tied to uncertainty estimates indicating the model confidence. The inner workings of Gaussian processes are exposed in details in the work of Rasmussen and Williams [31].

The use of Gaussian processes to model thermomechanical properties of the nickel-based polycrystalline superalloys, such as the yield strength, the ultimate tensile stress and the creep rupture stress has been known for two decades [3, 12, 32]. The predictions of such models have displayed good agreement with actual data from experimental validations [33, 34].

In this work, a Gaussian process-based model is generated to provide estimates of creep rupture stresses of the single crystal nickel-based superalloys as a function of their composition, the temperature and the envisioned time to rupture. To this end, data are gathered from the scientific and technical literature, including more than 300 patents. The resulting database is 1963 line long and contains the composition of 612 alloys as well as their creep testing settings and results (temperature, time and stress). The nature and boundaries of these inputs are detailed in Table 1. Both time to rupture and creep rupture stress are expressed in logarithmic units so that the distribution of data points is more uniform. The model is built using the Netlab library [35]. Compositions and properties were normalised between 0 and 1. A squared exponential kernel was employed [31], with its hyperparameters optimised using scaled conjugate gradients based on the logarithm of the likelihood.

Table 1: Nature and range of variables in the creep rupture stress database.

Input	Unit	Minimum	Maximum
Al		0.39	9
Co		0	17
Cr		0	16
~~Fe~~		~~0~~	~~5~~
Hf		0	2
Mo		0	13
Nb	wt.%	0	4
Re		0	11.5
Ru		0	9.7
Ta		0	12.1
Ti		0	5
~~V~~		~~0~~	~~4~~
W		0	18.6
Temperature	°C	650	1204
Time to rupture	log h	−0.90	4.32
Creep rupture stress	log MPa	1.15	2.99

Of note is the absence of heat treatments in the database. Instead, all alloys are considered to have an optimal microstructure when their creep lives are reported. Only when identical alloys were found in different sources is a choice made in favour of that displaying the highest resistance. This avoids the additional burden of dealing with incomplete reporting of heat treatment parameters or the difficulty of modelling the heat treatment effects. This indirect consideration is reasonable in that finding the right heat treatments for an alloy is easier than tuning its composition, as fewer variables are involved. Besides, as the proposed design procedure exploits to their best the conventional metallurgical routes, heat treating should closely resemble that of existing single crystal nickel-based superalloys.

Validation of the model is performed through five-fold

cross-validation, which consists in randomly splitting the database in five subsets of identical length, using four subsets to train the model and the fifth to test its predictive capabilities. The process iterates so that each of the subset is used for validation. The whole operation is repeated ten times over which three metrics are averaged: the Mean Absolute Error (MAE, Equation 1), the Mean Absolute Percentage Error (MAPE, Equation 2) and the Root Mean Square Error (RMSE, Equation 3). These metrics are based on the difference $e_i = y_i - y_i^*$ between the actual expected value y_i of the creep rupture stress and the corresponding prediction y_i^*.

$$\mathrm{MAE} = \frac{1}{N}\sum_{i=1}^{N}|e_i| \tag{1}$$

$$\mathrm{MAPE} = \frac{100}{N}\sum_{i=1}^{N}\left|\frac{e_i}{y_i}\right| \tag{2}$$

$$\mathrm{RMSE} = \sqrt{\frac{1}{N}\sum_{i=1}^{N}e_i^2} \tag{3}$$

with N the length of the database. While mathematically different, these metrics all provide insights into the generalisation capability of the model, i.e. its ability to correctly interpolate to unknown inputs which were not in the database used for training. Without loss of generality, the smaller their values, the better the predictive capability.

Five-fold cross-validation results in a MAE of 0.0280 log MPa (equivalent to an error of ±19 MPa on a estimate of 300 MPa), a MAPE of 1.26 % (±22 MPa) and a RMSE of 0.0548 log MPa (±38 MPa), which highlights a reasonable generalisation capability of the model.

Creep rupture stresses are evaluated at four temperatures and times representative of expected turbine loads: 1100 h at 950 °C, 110 h at 1050 °C, 550 h at 1050 °C and 510 h at 1200 °C.

3.2. Microstructure suitability

The CALPHAD method is used to evaluate the performance of the screened alloys on the basis of their constitution. The Thermo-Calc software [36] coupled with the thermodynamic databases TTNI8 [37] and TCNI9 [38] dedicated to nickel-based alloys is employed to estimate the equilibrium fractions of γ' and TCP phases and the composition of the (γ) matrix and γ' phase, which in turn serves in the computation of the γ/γ' lattice misfit.

The maximum allowed content of TCP phases is determined after computing the TCP content of actual alloys (listed in Figure 6) and comparing it with values reported in the literature. It is observed that a calculated content of 6 mol.% would lead to a much lower actual TCP phases fraction after long-time exposure at the same temperature, which is deemed adequate for long-term stability. Alloys featuring a calculated TCP phases content greater than 6 mol.% (whichever database is used) are thus rejected.

Table 2: Coefficients a_γ^i and $a_{\gamma'}^i$ used for the calculation of the lattice misfit according to Caron [39] or Kablov [40].

	γ phase (Å)		γ' phase (Å)	
	Caron	Kablov	Caron	Kablov
c	3.524	3.5219	3.57	3.5691
Al	0.179	0.221	0	0
Co	0.0196	0.059	−0.0042	−0.002
Cr	0.110	0.122	−0.004	0.014
Hf	1	1.559	0.7	1.339
Mo	0.478	0.412	0.208	0.097
Nb	0.7	0.595	0.46	0.275
Re	0.441	0.382	0.262	−0.504
Ru	0.3125	0.303	0.1335	0.083
Ta	0.7	0.693	0.5	0.398
Ti	0.422	0.302	0.258	0.149
W	0.444	0.435	0.194	0.151

3.2.1. Lattice misfit

The lattice parameters of the γ and γ' phases are computed following the methodology of Caron [39] and that of Kablov [40]:

$$a_j = c_j + \sum_i a_j^i x_j^i \tag{4}$$

where c_j is a constant and a_j^i and x_j^i are respectively the atomic fraction and the Vegard coefficient of element i in phase j (Table 2). The former is estimated with the help of Thermo-Calc. The lattice misfit δ is then calculated as

$$\delta = 2\frac{a_{\gamma'} - a_\gamma}{a_{\gamma'} + a_\gamma} \tag{5}$$

A slightly negative misfit is said to enhance the creep resistance [29].

3.2.2. Corrosion resistance

The resistance to corrosion of the single crystal nickel-based superalloys is typically imparted by additions of aluminium and chromium in quantities such that a protective layer of mixed oxides (including aluminium and chromium sesquioxides) can form. Its growth is impeded by possible depletion of both elements: aluminium in γ'

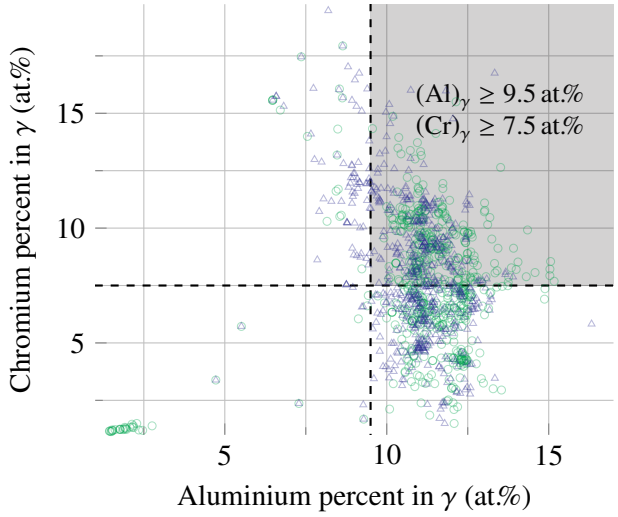

Figure 1: Equilibrium chromium content in γ at 1200 °C as a function of that of aluminium. Results from TTNI8 and TCNI9 are respectively drawn as circles and triangles.

precipitates and chromium in TCP phases. Environmental resistance can then be naively considered a direct function of the amount of these elements that remains free to diffuse outward, i.e. whose mobility is not mostly disabled by the formation of Al- and Cr-rich phases in the alloy. We thus relate corrosion resistance to the content of aluminium and chromium in the (γ) matrix.

Alloys from the creep rupture stress database are used to tune the minimal thresholds of aluminium and chromium by computing their equilibrium constitution at 1200 °C (Figure 1), at which the harshest rate of degradation by corrosion is expected. Following the composition of the (γ) matrix of CMSX-4, an alloy with satisfactory corrosion resistance currently used in commercial gas turbines, minima of 9.5 at.% Al and 7.5 at.% Cr are set. These minima are quite restrictive: if the alloys from the database were to be screened, 53 % (TTNI8) or 60 % (TCNI9) of them would be rejected (Figure 1).

3.2.3. *Processability*

Multiple heat treatments are used to control the size and distribution of γ' precipitates in the single crystal nickel-based superalloys. The success of these treatments ultimately depends on the possibility to solutionise the γ' phase while still in solid state, i.e. at a temperature lower than the alloy solidus. Equilibrium calculations are employed to ensure a difference Δ_S of at least 10 K between the solidus and the solutionising temperature.

Table 3: Coefficients of the volumetric mass density model (Equation 7).

Element	$a_i \times 10^3$
Ni	−1.49
Al	61.83
Co	3.66
Cr	1.21
Hf	86.33
Mo	−18.35
Nb	53.27
Re	1.60
Ru	12.64
Ta	10.81
Ti	48.58
W	4.57

3.3. *Castability: freckles resistance*

The susceptibility to Freckles Resistance (FR), a common casting defect, is estimated following the approach of Konter *et al.* [41]. Provided the relation described in Equation 6 is followed, the alloy is considered immune to freckling.

$$\frac{1.5w_{\mathrm{Hf}} + 0.5w_{\mathrm{Mo}} + w_{\mathrm{Ta}} - 0.5w_{\mathrm{Ti}}}{1.2w_{\mathrm{Re}} + w_{\mathrm{W}}} \geq 0.7 \qquad (6)$$

w_i being the nominal content of element i in wt.%.

3.4. *Volumetric mass density*

The reduction of volumetric mass density (ρ) increases the life of turbine blades by lowering the stresses induced by centrifugal forces.

The density is modelled following the approach of Hull [42] based on data previously gathered from the same literature search as the creep rupture stress (Equation 7). The database contains 210 measurements on 189 alloys, from single crystal, directionally solidified and polycrystalline cast or wrought families.

$$\rho = \frac{100}{\sum_i \frac{w_i}{\rho_i}} + \sum_i a_i w_i \qquad (7)$$

with ρ the alloy density in g.cm^{-3} provided w_i is the nominal content of element i in wt.% and ρ_i its density in g.cm^{-3}. The regression coefficients a_i are given in Table 3.

The density of alloys to be designed is limited in order to match that of common single crystal nickel-based superalloys such as CMSX-4+ and CMSX-10K. Given the model predictive error estimated by leave-one-out cross-validation is 0.05 g.cm^{-3}, a limit of 9.05 g.cm^{-3} is set; thus no alloy with an actual density between 8.95 and 9.00 g.cm^{-3} should be excluded.

Table 4: Boundaries of the explored space (wt.%).

Element	Minimum	Maximum
Al	4	8
Co	0	14
Cr	4	15
Hf	0	0.5
Mo	0	3
Nb	0	3
Re	0	6
Ru	0	2
Ta	5	15
Ti	0	3
W	0	10
C	0.02	

4. Results

This section exposes both the methodology and results of the models exploitation.

4.1. Search specifications

A systematic grid-search in the space defined in Table 4 is conducted. Each element is varied by steps of 1 wt.% with the exception of hafnium (0.5 wt.%). Nickel remains the balance element of every alloy. A 200 ppm carbon content is imposed to take into account its effect as a potential trace. The resulting search space contains about 293 million alloys (combinations). The explored area fits within the space covered in the CRS database, and the boundaries of alloying elements place the search space in the most densely populated area of the database.

The systematic screening allows for a more complete mapping of the compositional space than advanced methods such as genetic algorithms [2, 11, 32] or sequential quadratic programming [6] which by nature only partially sample it and hence do not provide an overall view of it. It also guarantees to find the optimal compositions in said space. Besides, the number of combinations in the present problem is such that the whole operation takes a reasonable amount of time.

The sequence of calculations is represented on Figure 2. Compared to Gaussian processes or empirical models, equilibrium calculations are time-consuming, taking up to 200 ms. The number of equilibria to compute is thus limited by pruning as much alloys from the search space as possible using the cheapest models first. The creep resistance is first evaluated using the Gaussian process-based model. Creep Rupture Stresses (CRS) are computed at four different temperatures and times: 950 °C / 1100 h, 1050 °C / 110 h, 1050 °C / 550 h and 1200 °C / 510 h. During the search, the alloys are judged based on the optimistic predictions, i.e. CRS nominal predictions augmented by one standard deviation (termed "augmented CRS" thereafter). That way, a larger number of alloys are kept than if the selection was done based on nominal predictions. This gives a measure of severity of the thresholds, and allows for a later fine-tuning of their value to study compromises required to select candidates with balanced properties. For every temperature-time couple, a threshold is set on this augmented CRS, accounting for specific applications of turbine blades: 300, 200, 150 and 55 MPa respectively. In total, 69 millions of the 293 million initial alloys pass this step.

The density is then computed, with 44 million alloys having a predicted density less than or equal to 9.05 $g.cm^{-3}$.

A first thermodynamic equilibrium calculation at 900 °C is done for every remaining alloys. Alloys featuring any phases besides γ, γ', carbides and TCP phases, or a TCP phases content exceeding 6 mol.%, are rejected. These calculations use the single equilibrium mode of Thermo-Calc, and result in about 40 million alloys being rejected, leaving approximately four million alloys for further evaluation.

The freckles resistance criterion disqualifies a further 500 000 alloys. The remaining alloys are screened for their corrosion resistance at 1200 °C (based on both Al and Cr content in their matrix) and then for their processability. To this end, equilibria are computed between 1300 °C and the solidus by steps of 10 K, with alloys still featuring γ' 10 K below the solidus being rejected.

At every temperature, the lattice misfits according to Caron and Kablov are calculated. In fact, no selection is necessary on their basis since their values are systematically below nought, whichever model is used.

The calculations use the TC Matlab Toolbox and are performed in parallel on all cores of a dual Xeon E5620 HP Z800 workstation. The whole exploration lasted 50 days. Both the TTNI8 and TCNI9 thermodynamic databases are used concurrently for all equilibrium computations.

4.2. Results

A total of 182 772 alloys out of 293 millions are found that follow the specifications laid in the previous section. These are termed "candidates" in the following discussion. According to predictions, these candidates should feature limited densities, good creep endurance, a dual phase γ/γ' microstructure with a negative lattice misfit, a limited TCP phases content, a good resistance to corrosion, a low susceptibility to freckling during casting and a window of

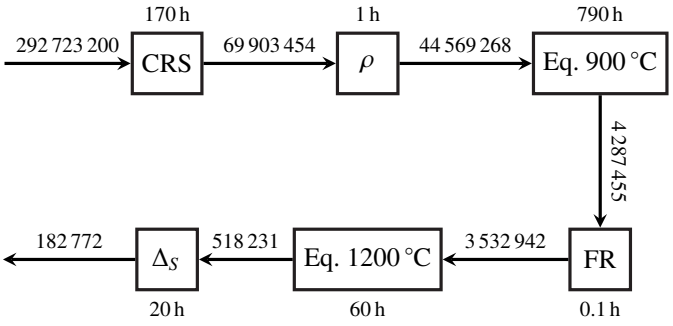

Figure 2: Sequence of calculation steps. Each box represents a calculation (see text for details). The approximate time taken to perform each calculation is associated with their respective box, with the number of alloys that pass the previous criterion indicated between each step.

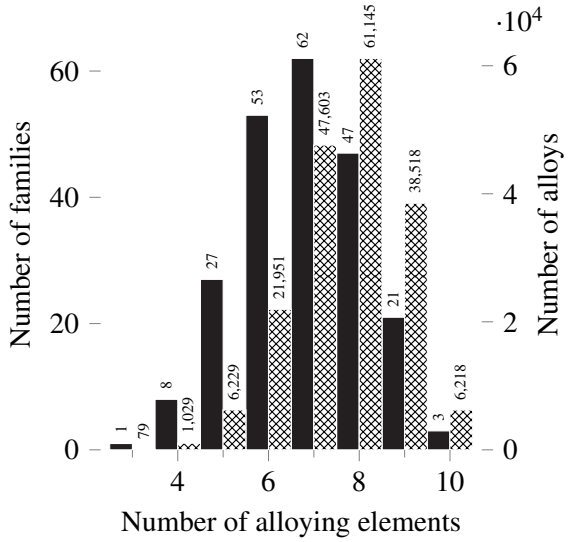

Figure 3: Number of families (filled bars) and corresponding number of alloys (crosshatched bars) classified according to the number of constitutive alloying elements.

solutionising of sufficient width.

These candidates belong to 222 alloy families (i.e. groups of alloys sharing identical alloying elements) of three to ten elements (Figure 3), which represent 11 % of the families that could be enumerated in the search space. Most alloys (81 %) possess seven to nine alloying elements.

Most used for alloying are aluminium, chromium and tantalum whose lower bounds are non-null (Figure 4). If one only considers the alloys with Al, Cr and Ta contents greater than their respective lower bounds, the first two elements remains the most used while significant additions of tantalum are only made in half the candidates. This behaviour is expected: Al is essential for the formation of γ' precipitates and higher Cr contents are mandatory to achieve the required content of this element in the γ matrix.

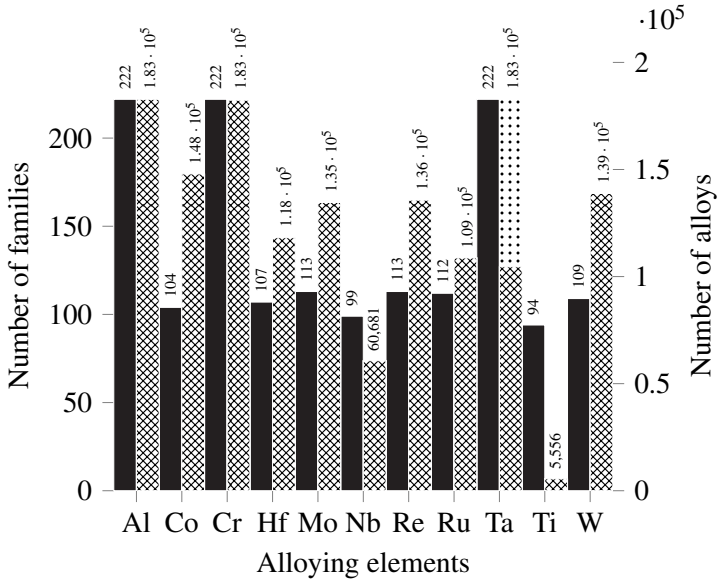

Figure 4: Number of families (filled bars) and corresponding number of alloys (crosshatched and dotted bars) containing the alloying element indicated on the abscissa. The dotted bar does not take into account the non-null lower bound of tantalum (see text for details).

Cobalt, tungsten, rhenium and molybdenum are present in at least 74 % of candidates. This contrasts with niobium and titanium whose representation in term of number of alloys is low despite their presence in a relatively high number of families and their ability to contribute to the formation of strengthening precipitates.

Whereas the search was conducted using augmented CRS predictions, the following sections make use of the "lowered CRS". The estimated CRS are lowered by one predictive standard deviation to ensure the robustness of the design procedure (i.e. minimise the risk of an alloy displaying lower than predicted properties). The distribution of predicted properties plotted on the side and bottom graphs of Figure 5 shows that the ranges of the lowered creep rupture stresses are large, spanning from tens to hundreds of megapascals, and that the density of candidates mostly lies between 8.4 and 8.7 g.cm^{-3}.

4.3. Comparison with existing alloys

It is important to note that, among the alloys from the creep rupture stress database (the "competitors"), none follows the microstructural specifications forced upon selected candidates, so that any direct comparison would be biased in favour of the competitors. Nevertheless, such a comparison is here attempted to illustrate the interest of the present alloy design strategy since, as will be shown, many candidates actually possess higher specific properties than competitors. In this aim, both populations are plotted

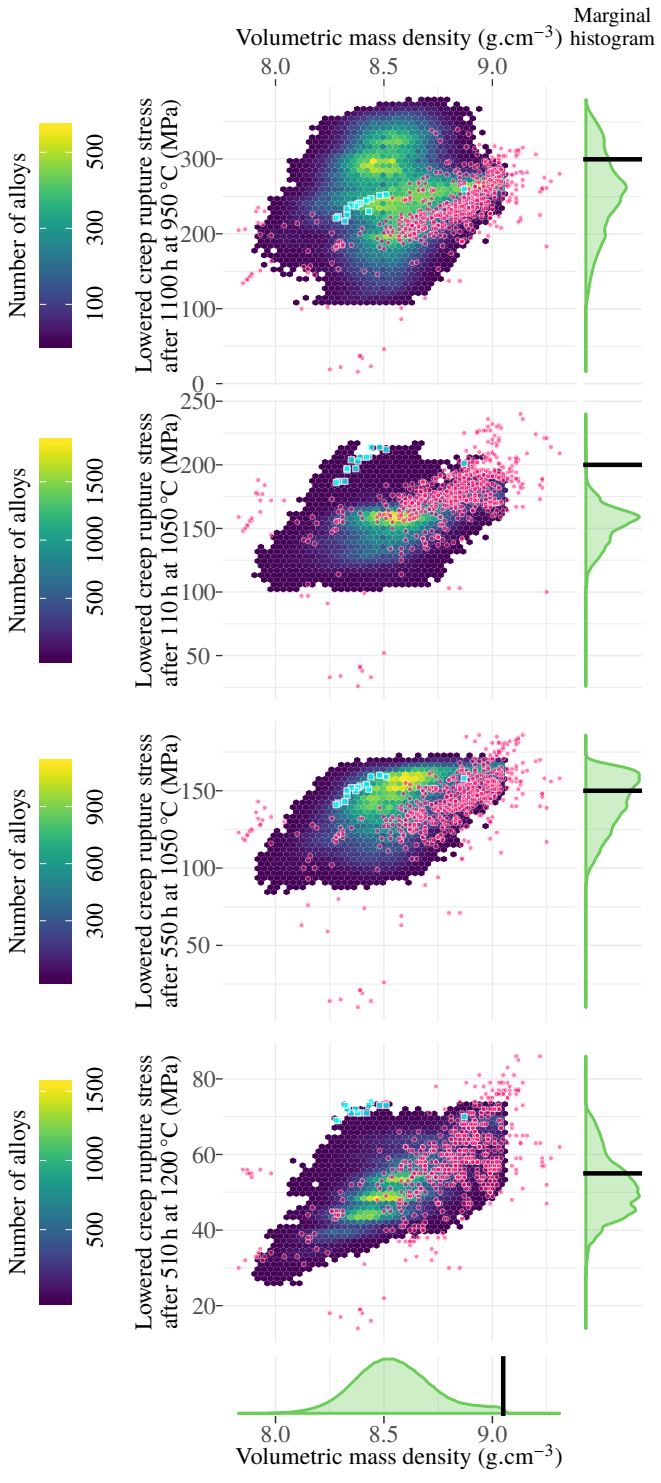

Figure 5: Lowered creep rupture stresses of candidates, competitors (pink dots) and candidates later selected (cyan squares) at 950, 1050 and 1200 °C as a function of their density. On the right side and bottom, the distribution of data points is given along the respective vertical and horizontal axis. (For interpretation of the references to colour in this figure legend, the reader is referred to the web version of this article.)

on Figure 5 as a function of their predicted density and predicted lowered creep rupture stresses. All plots share the same abscissa. Since the existing alloys were used to train the model, their predicted properties are close to their actual values.

As individual marks would make any plot difficult to interpret, the 182 772 candidates are regrouped in hexagons whose colour depends on the number of candidates lying within their boundaries (see left colour bars). Competitors are symbolised by pink dots. For each graph, the distribution of data points on the vertical axis (lowered creep rupture stresses) is given on the right hand side of the figure for the candidates. The same representation is available at the bottom of the figure, where the distribution of data points is given for the volumetric mass density. On each of the distribution plots, a black line symbolises the threshold from the search specifications (cf. subsection 4.1). ~~It is interesting to note that, with the exception of the 1050C / 110h creep conditions, there are candidates whose lowered resistances surpass the thresholds that were specified for augmented CRS during screening.~~

The range of lowered CRS for candidates and that of competitors largely overlap. However, subtracting one standard deviation from nominal CRS predictions reduces the CRS of candidates more than that of competitors: the predictive error is indeed smaller for the latter, which were used to train the models. This means there is a possibility of finding candidates with higher nominal CRS compared to competitors.

The population of candidates in the low-to-intermediate densities domain (between 8.0 and 8.5g/cm3) is significantly larger than that of competitors. The fact that, whatever the investigated temperatures and creep rupture times, candidates exhibit the highest lowered CRS in this domain is an achievement: since this domain is of particular interest for gas turbines, such alloys can be regarded as possessing optimal combinations of properties. This shift towards alloys displaying optimal sets of characteristics hints at the successful exploration of the design space.

A small number of competitors display higher lowered CRS at densities lower than 8g/cm3. These are however incomparable because none of them fulfills the relatively severe microstructural constraints enforced on candidates. Enforcing some of these specifications goes against the improvement of properties, but such limitations are not forced upon the competitors. As a matter of fact, none of them follow the combination of all specifications of section 3. This should make it more difficult to design new alloys respecting such constraints while possessing better properties than competitors. It is thus quite remarkable to find

candidates with similar or even higher predicted properties than competitors. It highlights that possibilities remain to improve the composition and microstructure of existing superalloys.

4.4. Selection of alloys for fabrication

Several alloys are selected in order to validate the design methodology. Suboptimal candidates are first ruled out: only alloys which are Pareto-optimal in terms of volumetric mass density and creep rupture stresses at all temperature are kept. By virtue of Pareto-optimality, no other alloy is stronger for a given density or lighter for a given resistance. Of the 182 772 candidates, 324 remain.

Fifteen candidates are then hand-picked according to the following criteria, linked to specifications in gas turbine design: (i) their calculated γ' content at 950 °C is between 60 and 80 mol.% and (ii) the ratio between their ~~predicted creep rupture stress~~lowered CRS at 1200 °C and their density is greater than 7 MPa.cm^3.g^{-1}.

The selection rely on predictions from both thermodynamics (for physical criteria) and Gaussian process regression (statistical) so as to ensure the consistency between the estimated microstructure and the estimated resistance to creep. This is to avoid the pitfall of selecting alloys with unrealistic microstructures when relying solely on a statistical model [22].

It was observed that CALPHAD predictions of TCP content using TTNI8 and TCNI9 were not equivalent, with difference ranging from 1mol.% to 40mol.%. These two computational thermodynamics databases mainly rely on the fitting of experimental data (as most CALPHAD databases do). It is thus not surprising to observe differences between their predictions for identical compositions. The selection process required an agreement between both (for all quantities computed using CALPHAD); having two databases with corroborating results minimises the risk of inadequate microstructure in the cast candidates.

The location of these fifteen candidates in comparison to competitors is shown on Figure 5 as cyan squares. They mostly do not overlap with competitors in these spaces of density and lowered creep resistance or are at the edges of their areas.

The major characteristics of one of the chosen candidates are graphically summarised on Figure 6. They are compared to the properties of some widely-used first- to fourth-generation single crystal nickel-based superalloys. For comparison purposes, the properties of the latter are computed using the models exposed in this paper.

The selected alloy displays the highest ~~predicted creep rupture stress~~lowered CRS at 1200 °C while those at 950 and 1050 °C remains excellent compared to the competition. This is however achieved at a much lower density: as much as 7 % is gained on CMSX-4+ and CMSX-10K, 5 % on CMSX-4 and 3 % on AM1. Its resistance to oxidation and corrosion should be better thanks to greater content of aluminium and chromium in its (γ) matrix, while its processability should be in-line with that of CMSX-4+ and CMSX-10K.

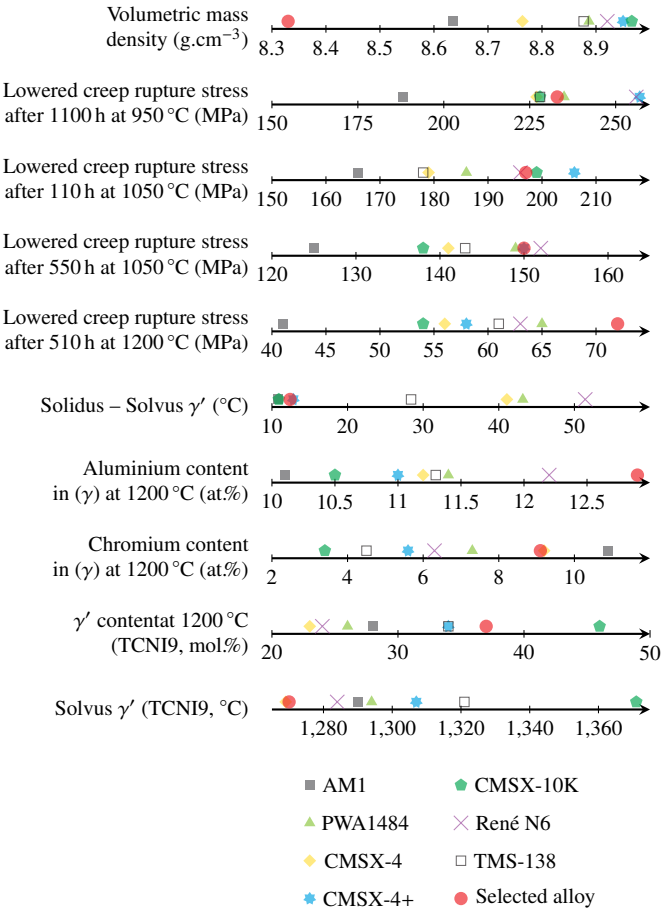

Figure 6: Comparison of the properties of the selected alloy (red disc) with those of popular alternatives.

The experimental characterisation of the selected alloys is on-going.

5. Conclusion

The combination of data mining models and computational thermodynamics brought to light the existence, in the large uncharted space of all superalloys, of a margin of improvement of the single crystal nickel-based superalloys. The search formed the basis of the isolation of thousands of superalloys which resulted in a 99.9999 % reduction of the space of possibilities. It led to the design of optimised alloys of higher predicted specific creep resistance

than current competitors. This is all the more remarkable that the search specifications included harsh microstructural constraints, which once more highlights the potential of such screening method to guide alloy design towards desirable compositional regions.

6. Data availability

The processed data required to reproduce these findings cannot be shared at this time due to legal or ethical reasons.

References

[1] K. Harris and J. B. Wahl. High strength single crystal nickel based superalloy, Patent EP2942411, 2014.

[2] M. Mahfouf. Optimal design of alloy steels using genetic algorithms. In *Advances in Computational Intelligence and Learning: Methods and Applications*, pages 425–436. Springer Netherlands, Dordrecht, 2002.

[3] F. Tancret, H. K. D. H. Bhadeshia, and D. J. C. MacKay. Design of a creep resistant nickel base superalloy for power plant applications: Part 1 — Mechanical properties modelling. *Materials Science and Technology*, 19:283–290, 2003.

[4] I. N. Egorov-Yegorov and G. S. Dulikravich. Chemical Composition Design of Superalloys for Maximum Stress, Temperature, and Time-to-Rupture Using Self-Adapting Response Surface Optimization. *Materials and Manufacturing Processes*, 20:569–590, 2005.

[5] W. Xu and S. van der Zwaag. Property and Cost Optimisation of Novel UHS Stainless Steels via a Genetic Alloy Design Approach. *ISIJ International*, 51:1005–1010, 2011.

[6] R. Rettig, N. C. Ritter, H. E. Helmer, S. Neumeier, and R. F. Singer. Single-crystal nickel-based superalloys developed by numerical multi-criteria optimization techniques: design based on thermodynamic calculations and experimental validation. *Modelling and Simulation in Materials Science and Engineering*, 23, 2015. 035004.

[7] B. D. Conduit, N. G. Jones, H. J. Stone, and G. J. Conduit. Design of a nickel-base superalloy using a neural network. *Materials & Design*, 131:358–365, 2017.

[8] W. Xu, P. E. J. Rivera-Díaz-del-Castillo, and S. van der Zwaag. Designing nanoprecipitation strengthened UHS stainless steels combining genetic algorithms and thermodynamics. *Computational Materials Science*, 44:678–689, 2008.

[9] R. C. Reed, T. Tao, and N. Warnken. Alloys-By-Design: Application to nickel-based single crystal superalloys. *Acta Materialia*, 57:5898–5913, 2009.

[10] P. E. J. Rivera-Díaz-del-Castillo and W. Xu. Heat Treatment and Composition Optimization of Nanoprecipitation Hardened Alloys. *Materials and Manufacturing Processes*, 26:375–381, 2011.

[11] F. Tancret. Computational thermodynamics and genetic algorithms to design affordable γ'-strengthened nickel-iron based superalloys. *Modelling and Simulation in Materials Science and Engineering*, 20, 2012. 045012.

[12] F. Tancret. Computational thermodynamics, Gaussian processes and genetic algorithms: combined tools to design new alloys. *Modelling and Simulation in Materials Science and Engineering*, 21, 2013. 045013.

[13] Q. Lu, S. van der Zwaag, and W. Xu. High-throughput design of low-activation, high-strength creep-resistant steels for nuclear-reactor applications. *Journal of Nuclear Materials*, 469:217–222, 2016.

[14] R.C. Reed, Z. Zhu, A. Sato, and D.J. Crudden. Isolation and testing of new single crystal superalloys using alloys-by-design method. *Materials Science and Engineering: A*, 667:261–278.

[15] M. Mahfouf, M. Jamei, and D. A. Linkens. Optimal Design of Alloy Steels Using Multiobjective Genetic Algorithms. *Materials and Manufacturing Processes*, 20:553–567, 2005.

[16] P. Das, S. Mukherjee, S. Ganguly, B. K. Bhattacharyay, and S. Datta. Genetic algorithm based optimization for multi-physical properties of HSLA steel through hybridization of neural network and desirability function. *Computational Materials Science*, 45:104–110, 2009.

[17] Q. Zhang and M. Mahfouf. A nature-inspired multi-objective optimisation strategy based on a new reduced space searching algorithm for the design of alloy steels. *Engineering Applications of Artificial Intelligence*, 23:660–675, 2010.

[18] S. Bhargava, G. S. Dulikravich, G. S. Murty, A. Agarwal, and M. J. Colaço. Stress Corrosion Cracking Resistant Aluminum Alloys: Optimizing Concentrations of Alloying Elements and Tempering. *Materials and Manufacturing Processes*, 26:363–374, 2011.

[19] Y. Sun, W. D. Zeng, Y. F. Han, X. Ma, and Y. Q. Zhao. Optimization of chemical composition for TC11 titanium alloy based on artificial neural network and genetic algorithm. *Computational Materials Science*, 50:1064–1069, 2011.

[20] A. Kumar, D. Chakrabarti, and N. Chakraborti. Data-Driven Pareto Optimization for Microalloyed Steels Using Genetic Algorithms. *Steel Research International*, 83:169–174, 2012.

[21] David J Crudden, Babak Raeisinia, Nils Warnken, and Roger C Reed. Analysis of the chemistry of Ni-base turbine disk superalloys using an alloys-by-design modeling approach. *Metallurgical and Materials Transactions A*, 44:2418–2430, 2013.

[22] R. Jha, F. Pettersson, G. S. Dulikravich, H. Saxen, and N. Chakraborti. Evolutionary Design of Nickel-Based Superalloys Using Data-Driven Genetic Algorithms and Related Strategies. *Materials and Manufacturing Processes*, 30:488–510, 2015.

[23] S. Dey, S. Ganguly, and S. Datta. In silico design of high strength aluminium alloy using multi-objective GA. In *Swarm, Evolutionary, and Memetic Computing: 5th International Conference (SEMCCO 2014)*, pages 316–327. Springer International Publishing, 2015.

[24] S. Pattanayak, S. Dey, S. Chatterjee, S. G. Chowdhury, and S. Datta. Computational intelligence based designing of microalloyed pipeline steel. *Computational Materials Science*, 104:60–68, 2015.

[25] N. S. Reddy, J. Krishnaiah, H. B. Young, and J. S. Lee. Design of medium carbon steels by computational intelligence techniques. *Computational Materials Science*, 101:120–126, 2015.

[26] Y.-K. Kim, D. K., H.-K. Kim, C.-S. Oh, and B.-J. Lee. An intermediate temperature creep model for ni-based superalloys. *International Journal of Plasticity*, 79:153–175, 2016.

[27] S. Sulzer and R Reed. Critical assessment 31: on the modelling of tertiary creep in single-crystal superalloys. *Materials Science and Technology*, 34(18):2174–2201, 2018.

[28] T. Murakumo, Y. Koizumi, K. Kobayashi, and H. Harada. Creep Strength of Ni-Base Single-Crystal Superalloys on the γ/γ' Tie-Line. In *Superalloys 2004 (Tenth International Symposium)*, Warrendale, PA, 2004. The Minerals, Metals and Materials Society.

[29] R. C. Reed. *The Superalloys: Fundamentals and Applications*. Cambridge University Press, Cambridge, 2006.

[30] D. K. Duvenaud. *Automatic Model Construction with Gaussian Processes*. PhD thesis, Pembroke College, University of Cambridge, 2014.

[31] C. E. Rasmussen and C. K. I. Williams. *Gaussian processes for machine learning*. The MIT Press, Cambridge, 2006.

[32] E. Menou, G. Ramstein, E. Bertrand, and F. Tancret. Multi-objective constrained design of nickel-base superalloys using data mining- and thermodynamics-driven genetic algorithms. *Modelling and Simulation in Materials Science and Engineering*, 24, 2016. 055001.

[33] F. Tancret, T. Sourmail, M. A. Yescas, R. W. Evans, C. McAleese, L. Singh, T. Smeeton, and H. K. D. H. Bhadeshia. Design of a creep resistant nickel base superalloy for power plant applications: Part 3 — Experimental results. *Materials Science and Technology*, 19:296–302, 2003.

[34] F. Tancret and M. Bellini. Properties, processability and weldability of a novel affordable creep resistant nickel base superalloy. *Materials Science and Technology*, 24:479–487, 2008.

[35] I. Nabney. NETLAB*: Algorithms for Pattern Recognition*. Springer, New York, 2002.

[36] *Thermo-Calc Software AB*. Online: http://www.thermocalc.com/ (last visited 12/03/2019).

[37] *Thermotech TTNI8 Ni-based Superalloys Database version 8*. Online: http://www.thermocalc.com/media/5980/dbd_ttni8_bh.pdf (last visited 12/03/2019).

[38] *Thermo-Calc Software TCNI9 Ni-based Superalloys Database version 9*. Online: https://www.thermocalc.com/media/83726/TCNI9_extended_info.pdf (last visited 12/03/2019).

[39] P. Caron. High γ' solvus new generation nickel-based superalloys for single crystal turbine blade applications. In *Superalloys 2000 (Ninth International Symposium),*, pages 737–746. The Minerals, Metals and Materials Society, 2000.

[40] E. N. Kablov and N. V. Petrushin. Designing of high-rhemium single cristal ni-based supealloy for gas turbine blades. In *Superalloys 2008 (Eleventh International Symposium)*, pages 901–908. The Minerals, Metals and Materials Society, 2008.

[41] M. Konter, M. Newnham, and C. Tonnes. Nickel-base superalloy, Patent US 5888451 A. 1999.

[42] F. C. Hull. Estimating Alloy Densities. *Metal Progress*, 59:139–140, 1969.

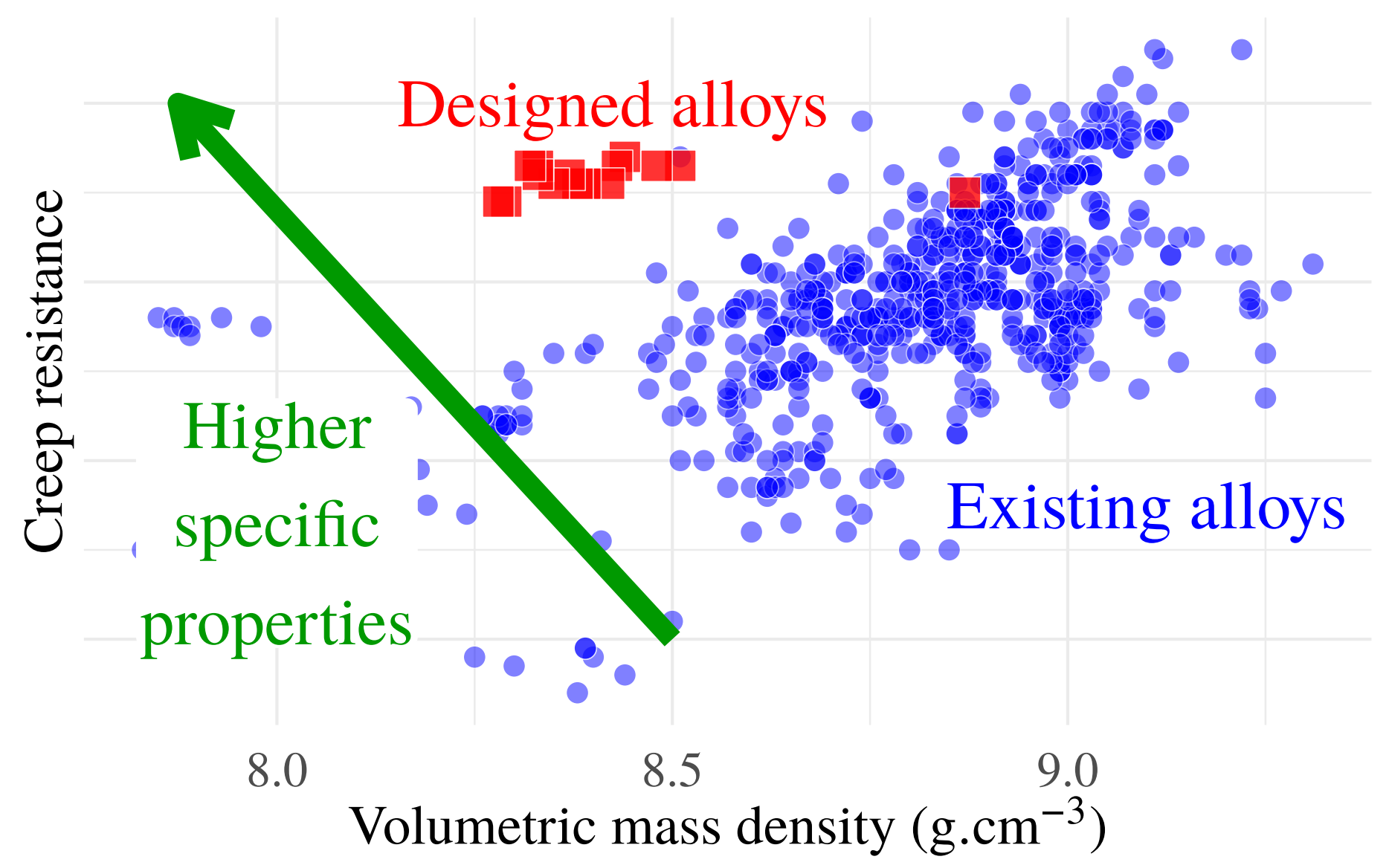
Designed alloys
Higher
specific
properties
Existing alloys
Creep resistance
8.0
8.5
9.0
Volumetric mass density (g.cm^{-3})